# Structure and Nature of Manganese(II) Imidazole Complexes in Frozen Aqueous Solutions

Sun Un*

Service de Bioénergétique, Biologie Structurale et Mécanismes (CNRS/UMR-8221), Institut de Biologie et de Technologies de Saclay, CEA-Saclay, 91191 Gif-sur-Yvette, France

S *Supporting Information*

ABSTRACT: A common feature of a large majority of the manganese metalloenzymes, as well as many synthetic biomimetic complexes, is the bonding between the manganese ion and imidazoles. This interaction was studied by examining the nature and structure of manganese(II) imidazole complexes in frozen aqueous solutions using 285 GHz high magnet-field continuous-wave electron paramagnetic resonance (cw-HFEPR) and 95 GHz pulsed electron–nuclear double resonance (ENDOR) and pulsed electron-double resonance detected nuclear magnetic resonance (PELDOR-NMR). The ^{55}Mn hyperfine coupling and isotropic g values of Mn^{II} in frozen imidazole solutions continuously decreased with increasing imidazole concentration. ENDOR and PELDOR-NMR measurements demonstrated that the structural basis for this behavior arose from the imidazole concentration-dependent distribution of three six-coordinate and two four-coordinate species: $[Mn(H_2O)_6]^{2+}$, $[Mn(imidazole)(H_2O)_5]^{2+}$, $[Mn(imidazole)_2(H_2O)_4]^{2+}$, $[Mn(imidazole)_3(H_2O)]^{2+}$, and $[Mn(imidazole)_4]^{2+}$. The hyperfine and g values of manganese proteins were also fully consistent with this imidazole effect. Density functional theory methods were used to calculate the structures, spin and charge densities, and hyperfine couplings of a number of different manganese imidazole complexes. The use of density functional theory with large exact-exchange admixture calculations gave isotropic ^{55}Mn hyperfine couplings that were semiquantitative and of predictive value. The results show that the covalency of the Mn–N bonds play an important role in determining not only magnetic spin parameters but also the structure of the metal binding site. The relationship between the isotropic ^{55}Mn hyperfine value and the number of imidazole ligands provides a quick and easy test for determining whether a protein binds an Mn^{II} ion using histidine residues and, if so, how many are involved. Application of this method shows that as much as 40% of the Mn^{II} ions in *Deinococcus radiodurans* are ligated to two histidines (Tabares, L. C.; Un, S. *J. Biol. Chem* **2013**, in press).
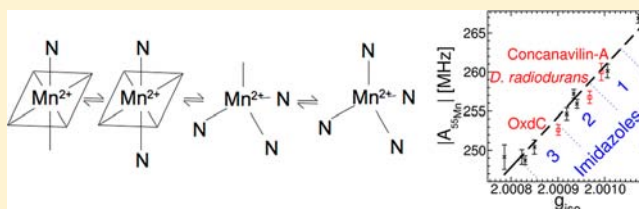
INTRODUCTION

In the Protein Databank, there are a nearly 1700 metalloenzymes that have manganese. These ions play a wide variety of functions. Some, like those in manganese superoxide dismutases (MnSOD) and the oxygen-evolving complex of the photosynthetic reaction center, are redox-active, while others play purely structural roles, as in Concanavilin-A (ConA). About two-thirds of these proteins use at least one histidine to bind the metal.[1] In *Deinococcus radiodurans*, a bacteria that can accumulate as much as 30 mM manganese,[2] a large portion of the Mn^{2+} ion is eventually incorporated into MnSOD and a metallopeptide or -protein that has yet to be identified.[3] This latter species was found to have a distinct high-field electron paramagnetic resonance (HFEPR) spectrum that could be mimicked by Mn^{II} in a frozen aqueous solution of imidazole (Figure 1). None of the common cellular metabolites (for example, phosphates) or simple free amino acids, including free histidine, produced a similar Mn^{II} HFEPR spectrum under physiological conditions. This suggested that the *D. radiodurans* species arose from a Mn^{II} ion bound to one or more histidine imidazole groups of a peptide or protein. A review of the existing data revealed that the differences in the EPR spectra of

Mn^{II}-binding proteins could be, in part, understood in terms of manganese–histidine ligation. The fifth resonance of the distinct sharp six-line Mn^{II} HFEPR spectra of these proteins coincided at nearly the same magnetic-field position, and the separation between the resonances, the ^{55}Mn hyperfine coupling (see below), appeared to depend on the number of ligating histidines. This can be seen in Figure 1, where the progression toward smaller hyperfine coupling from $[Mn(H_2O)_6]^{2+}$ to ConA, which has one histidine in its manganese binding site,[4] to oxalate decarboxylase (OxdC), which has three (high-pH form of the "site-1"),[5,6] is evident. Intermediate between the last two was the stationary-phase *D. radiodurans* spectrum. This variation in the magnetic spin parameters caused by Mn^{II}–imidazole bonding meant that the electronic structures of the metal centers were being strongly affected. In order to understand these effects more quantitatively, we examined the nature and structure of manganese(II) imidazole complexes in frozen aqueous solutions.
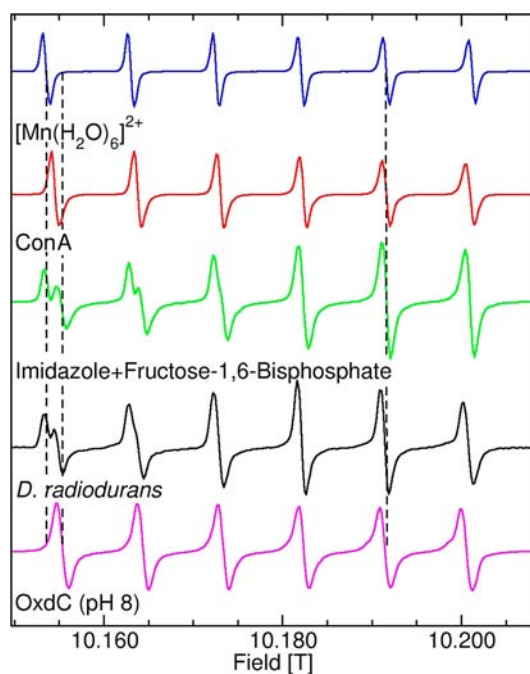
Figure 1. Comparison of the 285 GHz cw-HFEPR Mn^{II} spectra of intact stationary-phase *D. radiodurans* cells (black) with pH 8 OxdC (magneta), coaxially mounted separate pH 7 samples of 50 μM Mn^{II} in 32 mM imidazole and 50 μM Mn^{II} in 100 mM fructose-1,6-bis(phosphate) (green), ConA (red), and 50 μM Mn^{II} in a 20% glycerol water solution (blue). See the text and ref 3 for details.

EPR methods can provide detailed information about both the electronic and physical structures of Mn^{II} centers. There are four principle magnetic spin interactions that define the EPR spectra of Mn^{II} ($S = {}^5/_2$ and $I[^{55}Mn] = {}^5/_2$): (1) the Zeeman interaction, the interaction of the electronic spin with the applied magnetic field, defined by the **g** matrix; (2) the zero-field interaction, defined by D and E values; (3) the electron–^{55}Mn nuclear hyperfine interaction internal to the Mn^{II} ion; (4) the electron–nuclear hyperfine interactions between the metal ion and surrounding magnetic nuclei. The latter two are defined by their respective **A** tensors. Together, the spin Hamiltonian that governs the EPR spectrum of a Mn^{II} ion is given by

$$H = \beta \vec{B} \cdot \mathbf{g} \cdot \vec{S} + \frac{D}{3}[3S_z^2 - S(S+1)] + \frac{E}{2}(S_z^2 - S_x^2)$$
$$+ \vec{S} \cdot (\mathbf{A}[^{55}Mn] \cdot \vec{I}_{55Mn} + \sum_n A_n \cdot \vec{I}_n)$$
$$+ [\vec{B} \cdot (\beta_{55Mn} \vec{I}_{55Mn} + \sum_n \beta_n \vec{I}_n)] \tag{1}$$

The nuclear Zeeman energies, the last term in eq 1, do not contribute to the EPR spectrum but are, nonetheless, important for the other techniques discussed below. In most cases, the ^{55}Mn hyperfine interaction (A^{55}_{Mn}) is essentially isotropic (and therefore we will use A^{55}_{Mn} to mean the isotropic ^{55}Mn hyperfine coupling constant), typically ranging from 160 to 300 MHz. To a nonrelativistic first-order approximation, the isotropic hyperfine coupling arises from the Fermi contact interaction, which depends on the spin density at the manganese nucleus. Its size has often been interpreted as reflecting the ionicity of the ligand manganese bonds.[7] The zero-field interaction reflect the symmetry of the ligand sphere,

being sensitive not only to the position and nature of the ligating atoms but also to the distribution of charges well beyond the primary ligand shell.[8] Typical pseudooctahedral six-coordinate Mn^{II} ions have zero-field interactions of less than 2 GHz. By comparison, little is known about the g values. Its range of values is very small from about 2.0007 to 2.0011, making systematic accurate measurements of the g values difficult.

When the magnetic field is sufficiently strong so that the Zeeman term is overwhelmingly dominant, eq 1 describes six electronic spin manifolds ($M_s = \pm^5/_2, \pm^3/_2, \pm^1/_2$), each composed of six submanifolds ($m_I = \pm^5/_2, \pm^3/_2, \pm^1/_2$) due to the ^{55}Mn nuclear moment, each of which, in turn, is further subdivided by other nuclear spins. The $M_s = -^1/_2 \leftrightarrow ^1/_2$ transition is unaffected to first-order in the magnetic field by the zero-field interaction.[9] Consequently, the spectrum of this transition for a typical six-coordinate Mn^{II} ion is simply composed of six sharp lines centered at $h\nu/g\beta$ and separated by $|A^{55}_{Mn}|$, making accurate measurements of both parameters possible.

It is possible to only populate the $M_s = -^5/_2$ electron spin state by using high magnetic-fields and low temperatures state and preferentially detect the spectrum of the $M_s = -^5/_2 \leftrightarrow -^3/_2$ transition. Such spectra are also centered at $h\nu/g\beta$, but in this case, their shapes are dominated by the zero-field interaction, providing a straightforward means for accurately determining of the zero-field D and E parameters.[6] It is also possible to determine these two parameters from the broadening induced by the higher-order effects of the zero-field interaction on the six $M_s = -^1/_2 \leftrightarrow ^1/_2$ resonances.[10,11]

The hyperfine interactions to ligand nuclei can provide a more detailed and nuanced picture of the structure and bonding interaction in the in vitro and in vivo manganese imidazole complexes but are generally too small to be measured directly from the cw-HFEPR spectra. However, they can be obtained using electron–nuclear double resonance (ENDOR) and electron pulsed double resonance detected nuclear magnetic resonance (PELDOR-NMR).[12] These techniques have been described in detail elsewhere.[12–14] ENDOR spectra have resonances at frequency positions given by[14]

$$\nu_{M_S}^{ENDOR} = \sqrt{(M_S A_{IS} - \nu_I)^2 + M_S^2 B^2}$$

$$A_{Is} = A_{IS,iso} + T(3\cos^2\theta - 1)$$

$$B = 3T\cos\theta\sin\theta \tag{2}$$

where ν_I is NMR frequency of nucleus I and T is the anisotropic component of the hyperfine interaction. In frozen solution spectra, the most intense resonances arise from $M_s = +^1/_2$ and $-^1/_2$ transitions. They occur pairwise, each having a line shape extending $^3/_2T$ (one from T to $-^1/_2T$ and the other from $^1/_2T$ to $-T$). The pair are offset from each other by A_{iso} and symmetrically centered about the NMR frequency of the nucleus (ν_I). The anisotropic components contain not only information about the angular orientation of the nuclei relative to the metal center but also about their distances because

$$T = \beta_n\beta_e / r^3$$

In practice, this dependence provides a simple, but very effective, means for discerning the Mn^{II} ligands. Water protons are typically about 2.9–3.0 Å from the metal center, while those (H_2 and H_5) of imidazoles (and histidines) that flank the

ligating nitrogen atom are about 3.4–3.5 Å. They correspond to $^3/_2 T$ values of 4.5 and 3.0 MHz, for the water and imidazole protons, respectively, making them readily distinguishable in the ENDOR spectra. The A_{iso} values for water protons are typically less than 1 MHz and those for H_2 and H_5 imidazole protons an order of magnitude less.[14] The A_{iso} values of other protons, for example, the two other protons on the imidazole ring, are essentially zero. ENDOR can also be used to determine the number of nuclei and ligands around the metal centers.[15,16]

PELDOR-NMR has been shown to be an effective method for detecting ^{14}N nuclei that are magnetically coupled to paramagnetic centers.[17,18] For transitions from the $M_s = -^1/_2 \leftrightarrow ^1/_2$ manifold, the PELDOR-NMR resonance frequencies to first-order in the magnetic field are given by

$$\nu_{M_S=-1/2\leftrightarrow1/2}^{PELDOR} = \begin{cases} \nu_S + \nu_I \pm \dfrac{1}{2}(A_{IS} - 3P) \\[2mm] \nu_S - \nu_I \pm \dfrac{1}{2}(A_{IS} + 3P) \end{cases}$$

(3)

where ν_I is the nuclear resonance frequency that for ^{14}N is 10 MHz when the EPR observation frequency, ν_S, is 94 GHz. The isotropic component ($A_{^{14}N,iso}$) of the hyperfine interaction (A_{IS}) between a Mn(II) ion and an imidazole nitrogen atom that bonds it is expected to be about 3 MHz and the nitrogen quadrupolar coupling (P) along the Mn−N bond about −1.5 MHz and 0.6 and 0.9 in the orthogonal directions.[19] Additional resonances from double-quantum transitions, as well as those from transitions between different Mn^{II} spin manifolds, will also be present in the spectra. The latter can be distinguished by their temperature dependence.

Using these techniques in conjunction with high magnetic fields, it was possible to measure accurately the Mn^{II} magnetic spin parameters of the imidazole complexes found in an aqueous solution. Density functional theory (DFT) calculations allowed us to put them into molecular and chemical context. This approach made it possible not only to determine the structure of these complexes but also to understand the nature of the Mn^{II}−imidazole bonding in them as well as in proteins.

■ EXPERIMENTAL SECTION

Unless otherwise specified, all aqueous solutions contained 50 μM manganese [from $Mn(ClO_4)_2\cdot6H_2O$], 100 mM NaCl, and 10−20% (v/v) glycerol and were between pH 6.8 and 7.2. All chemicals were used without further purification.

The 285 GHz cw-HFEPR spectra were obtained at 23 K with a modulation of 2 G under nonsaturating conditions on a locally constructed spectrometer.[20] The g_{iso} value of a manganese(II) solution containing only the components described above was 2.00107 (based on a Mn^{II}:Mg-to-O value of 2.00101[21]). The magnetic field at which the fifth hyperfine resonance crossed zero on four successive sweeps had a standard deviation of 3×10^{-5} or 7×10^{-6} in g. This solution was used as the field standard. It was placed in a sample tube that was coaxially mounted inside the larger sample holder that contained the sample of interest.

Commercial ConA (Sigma-Aldrich) was washed with 10 mM pH 7 HEPES and concentrated. The final sample also contained 150 mM NaCl. A comparison of optical and atomic absorption data indicated that about 20% of the Mn^{II} binding sites was occupied. The concentration of Mn^{II} was about 150 μM. The OxdC and *D. radiodurans* samples are described elsewhere.[3,6]

The 95 GHz ENDOR and PELDOR-NMR spectra were obtained at 6 K using a Bruker Elexsys II 680 EPR spectrometer equipped with a Bruker "power upgrade 2", a 500 W Amplifier Research radio-

frequency amplifier, and an Oxford Instruments CF935 flow cryostat. The Davies ENDOR[22] was obtained using an initial 200 ns microwave inversion pulse followed by a 20 μs radio-frequency excitation of the nuclear spins, and the detection was achieved using an echo detection comprised of 10 and 20 ns pulses. The PELDOR spectra were obtained by sweeping the frequency of a 90 μs "high-turn angle" (HTA) pulse followed by an echo detection using 120 and 240 ns pulses. At the detection frequency, $\omega_{1,HTA}$ was 2.1×10^6 rad/s, and at the ^{14}N resonance frequency, about 10 MHz from the detection frequency, $\omega_{1,HTA}$ was 1.3×10^6 rad/s. The PELDOR spectra were symmetrized about the detection frequency.

The ENDOR spectra were normalized to the integrated intensity of the ^{55}Mn ENDOR resonances (see the Supporting Information). Each PELDOR-NMR spectrum was normalized to the amplitude of the large center resonance. The power of the PELDOR-NMR HTA pulse was adjusted to be the same for all samples by ensuring that the echo shape and amplitude were the same when the frequency of the HTA and detection pulses were equal. Consequently, the widths of the center resonances for all samples were the same.

PELDOR-NMR and ENDOR spectra were obtained by exciting the highest-field Mn^{II} hyperfine line.

The *Gaussin09* program (revision B.01;[23] see the Supporting Information for the full citation) was used to carry out all density functional theory (DFT) calculations. The structures were first geometry-optimized using the B3LYP/6-31+G(D,P) DFT and basis-set combination. Normal-mode analysis was used to verify that the optimized structures were true energy minima. For ConA and OxdC, the calculations were restricted to the Mn^{II} center and the six primary ligands. The histidine ligands were replaced by imidazoles, and the glutamate was replaced by formate. The ConA model did not geometry-optimize correctly and the structure for subsequent calculations was based on the crystallographic coordinates (pdb code: 1NLS)[4] with hydrogen atoms at standard distances. Geometry optimization of the OxdC model was successful and was carried out with the molecule embedded in a solvent with a dielectric constant of 10. Natural population analysis[24] (NPA) charges for all models were determined using the B3LYP/6-31+G(D,P) combination. Different DFT and basis-set combinations were used to calculate the Mulliken spin densities and hyperfine couplings. Reported thermochemical values were calculated with the molecules embedded in water. Relativistic contributions to the hyperfine couplings were neglected.

■ RESULTS

As is apparent from Figure 2A, the spacing between the six resonances in the 285 GHz cw-HFEPR spectra of Mn^{II} in an imidazole buffer decreased with increasing imidazole concentration. Coincident with this decrease in $|A^{55}_{Mn}|$ was a decrease in g_{iso} in such a manner that the magnetic-field position of the fifth hyperfine line (10.193 T) remained nearly constant. The $|A^{55}_{Mn}|$ and g_{iso} values in Table 1 and Figure 3 were obtained by manually picking the zero-crossing points of each of the hyperfine resonances. The average of these field positions, $B_{average}$, corresponded to g_{iso} ($h\nu/\beta B_{average}$), and the average spacing between adjacent resonances was $|A^{55}_{Mn}|$. If one assumed that the statistical spread in the spacing was due to uncertainties in measuring the magnetic field, this amounted to about 0.5−1.5 G or about 15 ppm with respect to the magnetic field, meaning the g_{iso} values could be measured to five significant figures. This approach ignored the possibility of higher-order shifts due to the zero-field interactions, but as will be seen, the zero-field interactions of manganese(II) imidazole complexes are very small and these second-order effects were well below the uncertainty of the measurements. For imidazole concentrations of less than 1 M, the $|A^{55}_{Mn}|$ and g_{iso} values were linearly correlated (Figure 3). The values for ConA and the six-coordinate Mn^{II} site in OxdC at pH 8 were also consistent with
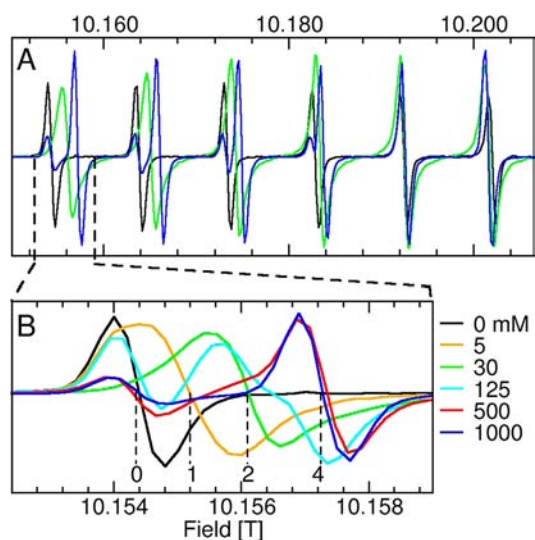
Figure 2. Dependence of the 285 GHz cw-HFEPR Mn^{II} spectra on the imidazole concentration: complete spectra (A) and expansion of the first hyperfine lines (B). The 125, 500, and 1000 mM spectra are examples of data obtained with a coaxially mounted $[Mn(H_2O)_6]^{2+}$ reference sample.

Table 1. Effect of the Imidazole Concentration on g_{iso} and $|A^{55}_{Mn}|$[a]

imidazole [mM]	g_{iso}[b]	$\|A^{55}_{Mn}\|$ [MHz]
0	2.00107	267
1	2.00108	266
5	2.00101	260
15	2.00093	257
31	2.00094	256
62	2.00092	255
125	2.00085	250
250	2.00083	249
500	2.00077	249
1000	2.00082	249
ConA pH 7	2.00099	259
OxdC pH 8	2.00090	253

[a]The uncertainties are ±0.00003 and 2 MHz, respectively. [b]Based on a Mn^{II}:MgO value of 2.00101.[21]

this correlation, as was the newly discovered *D. radiodurans* manganese species.[3]

The peak positions and line shapes of the lowest-field hyperfine resonances suggested that in the frozen manganese-(II) imidazole solutions, in addition to $[Mn(H_2O)_6]^{2+}$, there were at least three other different species. Their zero-crossing points are indicated in Figure 2B. Using this information as a starting point, a series of difference spectra were calculated from the imidazole titration data. In total, five components were identified (Figure 4A). Two of these corresponded to the spectra of the $[Mn(H_2O)_6]^{2+}$ and 1 M imidazole samples. Two more six-line spectra with simple line shapes were readily found, one dominating between 3 and 10 mM imidazole and the other between 20 and 100 mM (Figure 4A, blue and cyan, respectively). These corresponded to the zero-crossing points respectively labeled "1" and "2" in Figure 2B. When the latter component and the 1 M imidazole spectrum were subtracted from the 150 to 300 mM imidazole spectra, a fifth six-line spectra with a more complex line shape was isolated (Figure 4A, magenta). The spectrum of each of the five species was
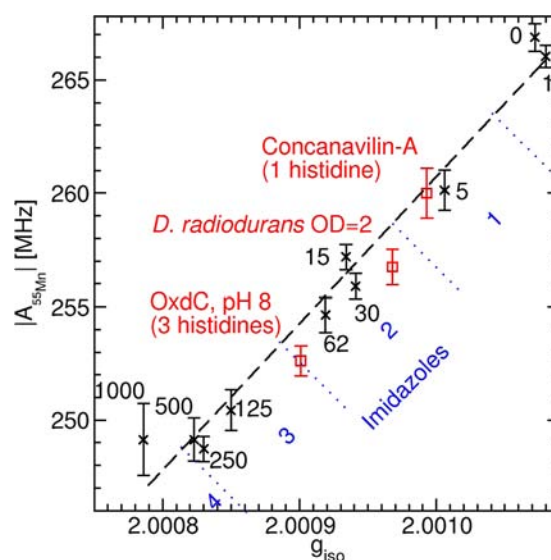

Figure 3. Relationship between the $|A^{55}_{Mn}|$ and g_{iso} values of 50 μM Mn^{II} as a function of imidazole concentration. OxdC and ConA g values were measured using the method described above. The errors represent the standard deviation in the separation of adjacent hyperfine lines. The dashed line is the linear regression fit. The imidazole concentrations are indicated in black and the approximate numbers of imidazole ligands in blue (see the text for details).

constructed using the average of several difference spectra obtained over the appropriate concentration ranges. Each was then normalized to its double integral. The resulting spectra were entirely consistent with the observation that the isotropic hyperfine and g values decreased with increasing imidazole concentration. The speciation of the five manganese(II) imidazole species (Figure 4C) was obtained by decomposing each spectrum of the titration series into the five components (Figure 4B) using linear regression analysis.

ENDOR and PELDOR-NMR were used to characterize the structures of these complexes and to examine the possible structural basis for trend isotropic g and hyperfine values. The proton ENDOR spectrum of $[Mn(H_2O)_6]^{2+}$ has been previously studied at 9 and 95 GHz.[25,26] The 95 GHz proton Davies ENDOR spectrum is shown in Figure 5A. In addition to the usual "matrix" resonances close to the ^{1}H NMR frequency (144.3 MHz) that correspond to distant protons, there were two other components: a large contribution with an $A^1_{H,iso}$ value of 0.89 and a $^3/_2T$ value of 4.91 MHz and a second smaller one with an $A^1_{H,iso}$ value of 0.05 and a $^3/_2T$ value of 0.87 MHz (Figure 5A). The first corresponded to a point–dipole distance of 2.89 Å consistent with the protons on ligating water molecules and the second to a solvation shell of surrounding protons with a Mn^{II}–^{1}H distance of 5 Å. The ENDOR spectrum of 50 μM Mn^{II} in 1 M imidazole had resonances that were considerably sharper than those of $[Mn(H_2O)_6]^{2+}$. This suggested that the positions of the protons in the imidazole complex were much more discrete. The spectrum also had two components. One had an $A^1_{H,iso}$ value of 0.0 MHz and a $^3/_2T$ value of 2.68 MHz (Figure 5A) or a point–dipole distance of 3.53 Å, consistent with the protons flanking the manganese-ligating nitrogen atom of the imidazole ring.[14] The outer extent of the second contribution was marked by the two features ±0.56 MHz about the ^{1}H NMR frequency (144.3 MHz) or a $^3/_2T$ value of 0.76 MHz assuming $A^1_{H,iso}$ was 0 MHz corresponding to a distance of 5.4 Å. This component
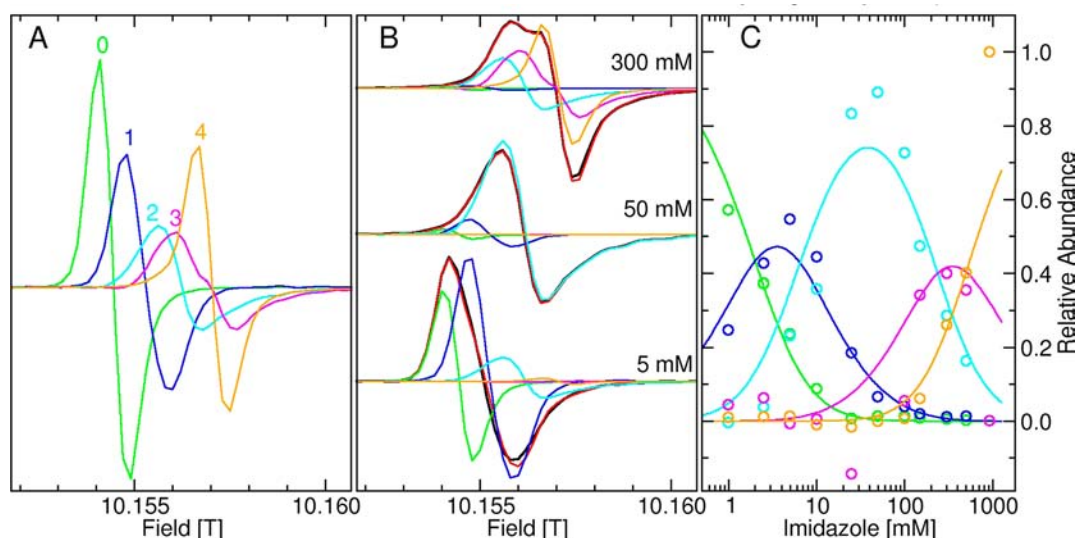
Figure 4. Speciation of manganese(II) imidazole complexes in frozen aqueous solutions determined by 285 GHz HFEPR: (A) normalized spectra of lowest-field hyperfine resonances of the five different species obtained from numerical decomposition; (B) linear regression fits of 5, 50, and 300 mM imidazole spectra using these five components; (C) relative concentrations of the five species (circles) from the fits in part B as a function the total imidazole concentration and manual fits of these speciation data based in Scheme 1 (solid traces). Experimental spectra are in black, linear regression fits in red, and the five components in green, blue, cyan, magenta, and orange. The differences in the 5 mM spectra in part C and Figure 1B (orange) show typical sample-to-sample variation. In all cases, the spectra have been normalized to their double integral.
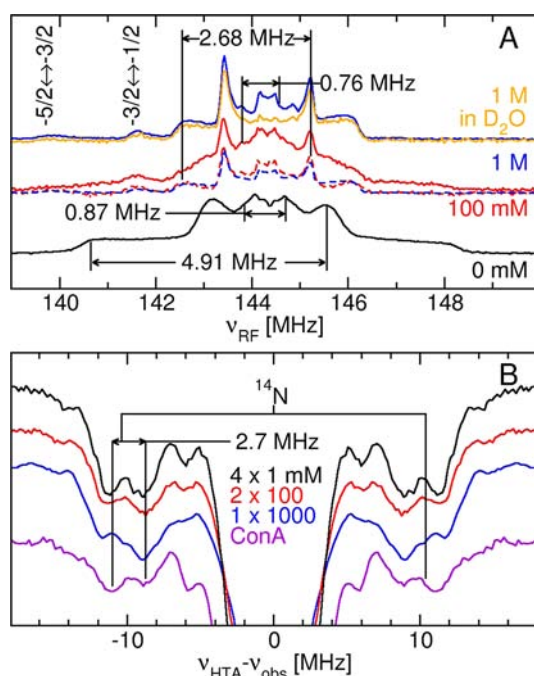

Figure 5. Mn^{II} 95 GHz proton ENDOR (A) and PELDOR-NMR (B) spectra as a function of the imidazole concentration. The ENDOR spectra were taken with 0 (black), 100 (red), and 1000 mM (blue in water and gold in D_2O) imidazole. The red dashed trace is the isolated imidazole component of the 100 mM spectrum (see the text for details), and the blue dashed trace is the 1000 mM spectrum scaled by 0.5. The indicated intervals in the ENDOR spectra correspond to the $^3/_2T$ value of the various components. The PELDOR-NMR spectra were taken with 1 (black), 100 (red), and 1000 mM (blue) imidazole and scaled by factors of 4, 2, and 1, respectively. A spectrum of ConA (purple) is shown for comparison. The ENDOR and PELDOR-NMR have been normalized as described in the Experimental Section.

disappeared, although not entirely, when the spectrum was obtained using D_2O (Figure 5A), indicating that it originated

from either protons from the surrounding solvent molecules or the distal N_3–H proton. The small remnant resonance may have resulted from incomplete deuterium exchange or the C_4–H proton, which is situated at a distance consistent with the T value. By variation of the temperature, it was also possible to assign the contributions from the $M_s = -^5/_2 \leftrightarrow -^3/_2$ and $-^3/_2 \leftrightarrow -^1/_2$ manifolds (Figure 5A).

The imidazole N–Mn^{II} hyperfine interaction was directly measured using PELDOR-NMR. These spectra showed a strong resonance at 10.4 MHz, the ^{14}N NMR frequency (Figure 5B). The overall shape of the spectra resembled that of ConA, which has a single imidazole in the Mn^{II} binding site. Both protein and frozen solution resonances were split by about 2.7 MHz. This value was close to the 3.2 MHz ^{14}N hyperfine coupling measured for Mn^{2+} doped in [Zn-(imidazole)$_6$]$^{2+}$ crystals (Mn:[Zn(imidazole)$_6$]$^{2+}$).[19]

The ENDOR spectrum of the 1 M imidazole complex did not extend beyond 146.5 MHz. This meant that the complex had no directly bound water ligands. For this reason, the spectrum was assigned to [Mn(imidazole)$_n$]$^{2+}$. The 95 GHz ENDOR spectra at intermediate imidazole concentrations could be readily decomposed into components resembling the [Mn(H_2O)$_6$]$^{2+}$ and [Mn(imidazole)$_n$]$^{2+}$ spectra (Figure 5A). The average numbers of water ligands were directly determined by a comparison of the relative intensity of the 147–148 MHz region of the normalized ENDOR spectra to that of [Mn(H_2O)$_6$]$^{2+}$. This approach was similar to that of Potapov and Goldfarb;[15] however, in our case, the spectra were first normalized to the ^{55}Mn ENDOR resonances (see the Supporting Information). The number of directly bound water ligands as a function of the imidazole concentration is shown in Figure 6. Using these results and the ENDOR spectrum of [Mn(H_2O)$_6$]$^{2+}$, it was possible to subtract the water contribution from the spectra, leaving the imidazole ligand component. An example is shown in Figure 5A for the 100 mM imidazole case. The difference spectra closely matched that of [Mn(imidazole)$_n$]$^{2+}$ with only small differences in the matrix
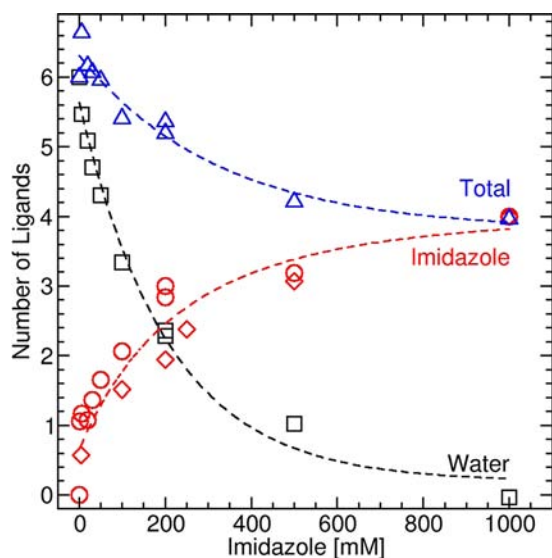
Figure 6. Number of water (black squares) and imidazole (red circles) ligands contributing to the ENDOR spectra as a function of the imidazole concentration and their sums (blue triangles). Also shown are the relative amplitudes of the ^{14}N PELDOR-NMR resonance (red diamonds) scaled to four imidazoles. The dashed lines show the trends in the data. See the text for details.

Figure 7. Isolated imidazole ENDOR spectrum of 50 μM Mn^{2+} in 1 and 20 mM imidazole solutions compared to that of the one-fourth-scaled spectrum of 50 μM Mn^{2+} in 1 M imidazole. A spectrum of one water ligand (one-sixth-scaled spectrum of $[Mn(H_2O)_6]^{2+}$) is also shown. All spectra have been normalized to the integrated intensity of the ^{55}Mn resonances.

resonances. The relative amplitude of the 0.76 MHz resonance remained unchanged, suggesting that it likely arose from the N_3-H proton rather than the solvent since one would expect the position of nearby solvent protons to change with variation in the number of imidazole ligands. The number of imidazole ligands relative to $[Mn(imidazole)_n]^{2+}$ was determined from the heights of the resonances at 143.4 and 145.3 MHz. Using this approach, the uncertainty in the number of water and imidazole ligands was estimated to be no bigger than 0.5. These results are summarized in Figure 6. The relative numbers of imidazole ligands obtained from the normalized PELDOR-NMR spectra were consistently slightly smaller than the ENDOR ones, although they were well within the estimated errors of the measurements (Figure 6).

Between 1 and 20 mM imidazole, the Mn^{II} ion had approximately 5.5 and 4.8 water ligands, respectively. Assuming all Mn^{II} centers in this concentration range were six-coordinate meant that there was about one imidazole per Mn^{II}. Figure 7 shows the isolated imidazole contribution to the 1 and 20 mM imidazole proton ENDOR spectra. As expected, the latter was slightly larger, but both were about one-quarter the intensity of the 1 M imidazole spectrum (Figure 7; see the Supporting Information for comparison to the one-sixth-scaled 1 M imidazole spectrum). Likewise, the intensity of the ^{14}N resonance of the 5 mM imidazole PELDOR-NMR spectrum was approximately one-quarter that of the 1 M spectrum (Figure 5B). This demonstrated that in the 1 M imidazole solution the Mn^{II} ions were four-coordinate with four imidazoles.

At 10 T and 4 K, the HFEPR spectrum of Mn^{II} ion is dominated by $M_s = -5/2 \leftrightarrow -3/2$ transitions.[6] This transition is essentially determined by zero-field interaction, providing an accurate and complete means for measuring the D and E values that characterize this interaction. The 4 K HFEPR spectra of $[Mn(H_2O)_6]^{2+}$ and $[Mn(imidazole)_4]^{2+}$ were narrow and featureless (Figure 8), indicating that the zero-field interactions were small and distributed. Consequently, only rough estimates
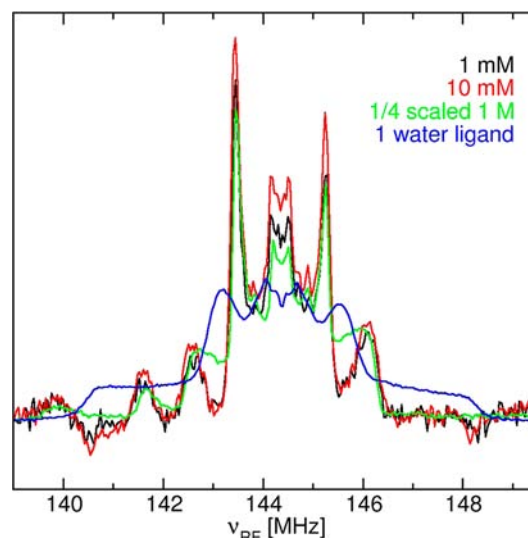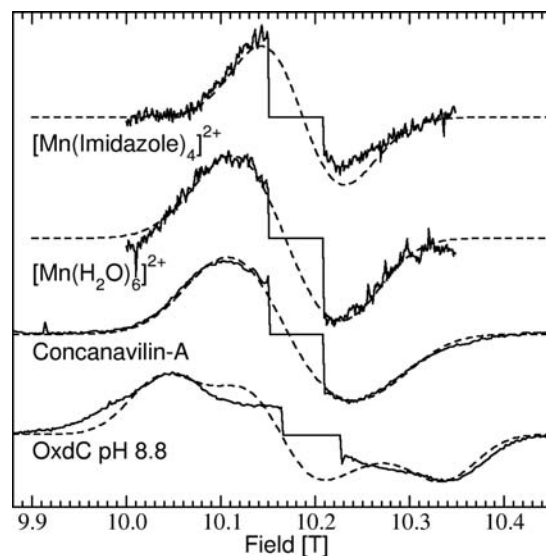

Figure 8. 285 GHz 4 K spectra of $[Mn(H_2O)_6]^{2+}$, $[Mn(imidazole)_4]^{2+}$, ConA and OxdC (pH 8.8). The region corresponding to the six $M_s = -1/2 \leftrightarrow +1/2$ transitions has been deleted for clarity. The dashed lines are simulations. The OxdC spectrum is the same as that previously reported.[6]

could be obtained from the simulations: $D = -160$ and $E = 0$ MHz for $[Mn(imidazole)_4]^{2+}$ and $D = -490$ and $E = 0$ MHz for $[Mn(H_2O)_6]^{2+}$; both were some of the smallest that we have measured. The two Mn^{II} centers in Mn:$[Zn(imidazole)_6]^{2+}$ had $D = -317$ and $E = -50$ MHz and $D = -354$ and $E = -66$ MHz.[19] By comparison, the manganese center in ConA (one imidazole) had $D = -630$ and $E = 160$ MHz and in OxdC (three imidazoles) $D = -1110$ and $E = 300$ MHz.[6] The simulations of the HFEPR data required Gaussian broadening of approximately 400 or 1 GHz (full width at half-height) to achieve reasonable fits. The distributions in either g or hyperfine values were unlikely to exceed the ranges covered

Table 2. Summary of Optimized Geometries Using the B3LYP/6-31+G(D,P) Functional and Basis Set[a]
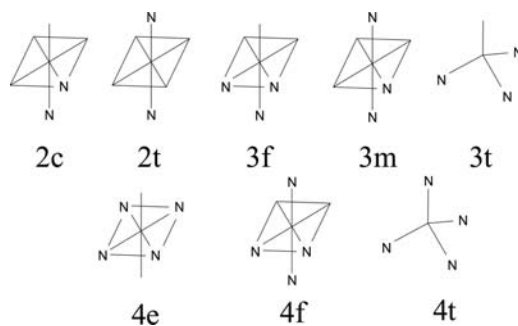
no. of imidazoles and geometry	average bond distances[b] (Å)			
	Mn−N$_1$ (imidazole)	Mn−H$_{2,5}$ (imidazole)	Mn−O (water)	Mn−H (water)
0			2.21	2.90 ± 0.01
1	2.15	3.37 ± 0.03	2.25 ± 0.01	2.93 ± 0.02
2t	2.19 ± 0.00	3.39 ± 0.03	2.30 ± 0.04	2.97 ± 0.03
2c	2.18 ± 0.01	3.39 ± 0.02	2.29 ± 0.03	2.97 ± 0.02
3m	2.22 ± 0.01	3.41 ± 0.03	2.33 ± 0.02	3.01 ± 0.02
3f	2.20 ± 0.00	3.40 ± 0.05	2.34 ± 0.00	3.02 ± 0.02
3t	2.11 ± 0.00	3.34 ± 0.04	2.20 ± 0.00	2.88 ± 0.01
4e	2.26 ± 0.02	3.45 ± 0.03	2.35 ± 0.02	3.02 ± 0.02
4e, experimental[c]	2.25 ± 0.04	3.39 ± 0.06	2.23 ± 0.00	2.72 ± 0.01
4f	2.24 ± 0.01	3.43 ± 0.02	2.40 ± 0.02	3.06 ± 0.05
4t	2.14 ± 0.00	3.35 ± 0.06		
5	2.28 ± 0.02	3.37 ± 0.09	2.47	3.13 ± 0.03
Mn[imidazole]$_6$, experimental[d]	2.27 ± 0.01	3.40 ± 0.05		

[a]The pictures show the positions of the imidazole nitrogen atom, with the rest of the positions being occupied by water. [b]The ranges denote maximum variation. [c]Experimental values from ref 31. The water protons are hydrogen bonded to nearby chlorides. [d]Experimental values from ref 30.

in Figure 3 and, therefore, too small to be responsible for the large distribution. This left only the zero-field interaction itself. Because the energy of the $M_s = -^5/_2 \leftrightarrow -^3/_2$ transitions is on the order of 4D, this meant that the zero-field interactions were distributed by at least 250 MHz, about the size of the ^{55}Mn hyperfine coupling. This large distribution was unlikely to be a consequence of structural disorder caused by the frozen aqueous environment. In the case of [Mn(imidazole)$_4$]$^{2+}$, the sharpness of the ENDOR resonances suggested that centers had a well-defined structure. More precisely, there was negligible distribution in the proton hyperfine interactions, in particular the dipolar couplings, which are determined by the Mn−H distances. Studies on single crystals of ConA have shown that the manganese ions occupy two sites that have different zero-field interactions (D = 789 and E = 189 MHz and D = 970 and E = 140 MHz) but the same proton ENDOR spectra, as well as ^{55}Mn quadrupole tensors.[27,28] This suggested that the Mn^{II} zero-field interactions are more sensitive than the other magnetic interactions to local structure disorder or, more likely, to nonstructural effects. Electrostatics originating from well beyond the primary ligand sphere have been shown to affect the Mn^{II} zero-field interaction with little or no change to the structure of the ligand sphere.[6,8] Therefore, it seemed likely that large zero-field distribution of the imidazole complexes originated from the disorder in the surrounding ions that did not affect the structure of the manganese imidazole complex. Interestingly, previous determinations of the zero-field parameters of ConA using analysis of the $M_s = -^1/_2 \leftrightarrow +^1/_2$ transitions were larger; for example, our values using multiple high-frequency data were D = 875 and E = 289 MHz, roughly the average of the single-crystal values. Measurements of the

zero-field parameters of [Mn(H$_2$O)$_6$]$^{2+}$ in 20% ethylene glycol obtained from spectral simulations yielded D = 610 and E = 0 MHz with unspecified minimal strain or distribution.[29] In both cases, the larger D values compared to the ones obtained directly from the $M_s = -^5/_2 \leftrightarrow -^3/_2$ spectrum likely reflects significant underestimation of the distribution. Unlike g and hyperfine interactions, there was no simple pattern to the variation in the zero-field parameters of these protein and complexes.

DFT calculations allowed us to put the EPR measurements into a molecular context. A total of 11 different structures of the form [Mn(imidazole)$_n$(H$_2$O)$_m$]$^{2+}$ (Table 2) were examined. Attempts at geometry optimization of [Mn(imidazole)$_6$]$^{2+}$ failed, with the outcome favoring a tetrahedral [Mn-(imidazole)$_4$]$^{2+}$ structure with two of the imidazole molecules completely displaced. [Mn(imidazole)$_6$]$^{2+}$[30] was only one of only two manganese(II) imidazole complexes found in the Cambridge Structure Database, with the other being [Mn-(imidazole)$_4$(H$_2$O)$_2$]$^{2+}$.[31] This suggested that in crystals additional forces may have been present to maintain the pseudooctahedral [Mn(imidazole)$_6$]$^{2+}$ structure. The DFT geometry optimization calculations of the mixed imidazole and water complexes resulted in stable six- and four-coordinate structures, although the structure of [Mn(imidazole)$_5$(H$_2$O)]$^{2+}$ had a significantly longer Mn−O distance (Table 2). The Mn−N ligand bond distance in the optimized [Mn-(imidazole)$_4$(H$_2$O)$_2$]$^{2+}$ structure with the water molecules in the trans configuration (structure 4t in Table 2) agreed with the crystal trans structure; however, the calculated Mn−O distances were significantly shorter, which was likely due to the hydrogen-bonding interactions of the water protons with
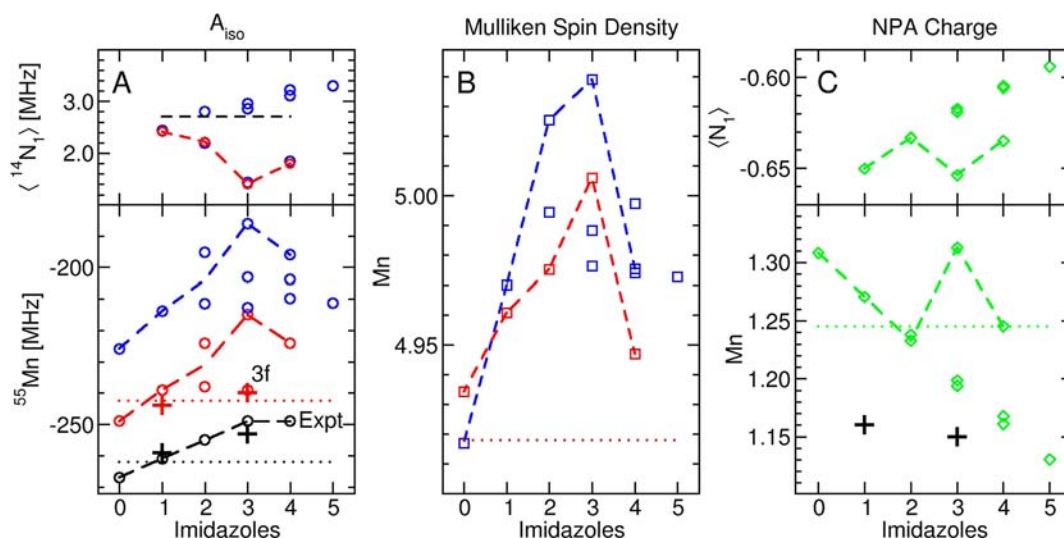
Figure 9. Calculated values as a function of imidazole ligation: (A) $A^{55}_{Mn,iso}$ and $A^{14}_{N,iso}$; (B) manganese Mulliken atomic spin densities; (C) manganese and nitrogen NPA charges. B3LYP/6-31+G(D,P) results are in green, B70LYP/9s7p4d/EPR-III in blue, and B95LYP/9s7p4d/EPR-III in red. Experimental $A^{55}_{Mn,iso}$ values are shown in black (circles and dashed lines). The dashed lines connecting the values correspond to the structures in Scheme 1. The values for ConA (one imidazoles) and OxdC (three imidazoles) are shown as plus signs. The dotted lines are the experimental (black) and calculated (red and green) values for $[Mn(PO_4H_2)(H_2O)_5]^+$. The nitrogen hyperfine couplings and charges are averages of only the ligated nitrogen atoms. Values for all structures are tabulated in the Supporting Information.

nearby chloride ions.[30] The relevant distances of the theoretical structures are summarized in Table 2.

The geometry-optimized DFT structures showed a trend toward longer Mn−H$_{water}$ with increasing number of imidazole ligands (Table 2), about 0.04 Å per imidazole or a decrease in the Mn^{II}−H dipolar coupling of about 100 kHz. This was consistent with the experimental data. The water component of the $[Mn(imidazole)_1(H_2O)_5]^{2+}$ ENDOR spectrum was subtly different from that of the $[Mn(H_2O)_6]^{2+}$ ENDOR spectrum. The difference spectra in Figure 7 had negative components relative to the $[Mn(imidazole)_4]^{2+}$ spectra at 140.5, 141.0, 145.5, and 148.3 MHz, the presence of which indicated that the water components in the imidazole complex spectra were slightly narrower than the spectrum of $[Mn(H_2O)_6]^{2+}$, with the difference in hyperfine coupling corresponding to about 60 kHz. By comparison, there were no measurable differences in the imidazole ENDOR contribution, consistent with the smaller dependence of the Mn−H$_{imidazole}$ distance on the number of imidazole ligands (+0.02 Å per imidazole).

The agreement between theory and experiment extended beyond the primary ligand sphere. Although we made no attempt to calculate the structure of the solvation shell around manganese(II) complexes, existing hybrid quantum mechanical/molecular mechanical calculations predict that the hydration sphere contains 51 protons at a distance of 4.9−6.0 Å from the Mn^{II} center.[32] This compared exceeding well with the Mn^{II}−^{1}H distance of 5 Å for solvent protons obtained from the 0.63 MHz coupling seen in the $[Mn(H_2O)_6]^{2+}$ ENDOR spectra.

The Mulliken atomic spin densities, NPA charges, and isotropic hyperfine couplings based on the optimized structure are summarized in Figure 9. The NPA Mn^{II} charges of the six-coordinate complexes linearly decreased with increasing imidazole ligation starting from 1.31 with no imidazoles to 1.13 with five imidazoles. The nitrogen charges increased, with the two four-coordinate structures being outliers. NPA Mn^{II} charges of $[Mn(PO_4H_2)(H_2O)_5]^{1+}$ and $[Mn(CH_3COO)(H_2O)_5]^{1+}$ were also calculated and found to be 1.24 and

1.25, respectively, the same as that for $[Mn(imidazole)_4]^{2+}$. The manganese spin densities of the six-coordinate models showed a general increasing trend. The two four-coordinate structures had the lowest manganese spin densities and were again outliers. The phosphate and acetate complexes had Mn^{II} spin densities of 4.84, the same as that of $[Mn(H_2O)_6]^{2+}$. The A^{55}_{Mn} and average ^{14}N hyperfine coupling constants were calculated using (1) the TPSSh/aug-cc-pVTZ-J DFT and basis set, as described by Hedegård and co-workers[33] and (2) the user-defined B70LYP (with 70% exact exchange and 30% $E_{XSlater}$ and 30% ΔE_{xB88} and E_{cLYP}) and B95LYP (with 95% exact exchange and 5% $E_{XSlater}$ and 5% ΔE_{xB88} and E_{cLYP}) hybrid functionals in conjunction with the 9s7p4d basis set for manganese, as described by Schinzel and co-workers,[34] except with the EPR-III basis set for the lighter atoms instead of the IGLO-III basis. For the latter method, spin contaminations due to the large exact-exchange admixtures were not excessive and no larger than those using B3LYP. For B95LYP, $\langle S^2 \rangle$ was 8.752 for $[Mn(H_2O)_6]^{2+}$ and 8.755 for $[Mn(imidazole)_4]^{2+}$ compared to the B3LYP values of 8.752 and 8.758 and the TPSSh values of 8.753 and 8.758, respectively. All three functionals underestimated the size of the ^{55}Mn isotropic coupling. The TPSSh/aug-cc-pVTZ-J approach gave the largest discrepancy, −189 MHz for $[Mn(H_2O)_6]^{2+}$ and −140 MHz for $[Mn(imidazole)_4]^{2+}$ compared to the experimental values of −267 and −249 MHz, respectively. The B95LYP hyperfine values were offset by less than +30 MHz from the experimental ones (Figure 9). This was true for the values of other centers as well, including those of ConA and OxdC. The B95LYP A^{55}_{Mn} value for $[Mn(PO_4H_2)(H_2O)_5]^+$ was 243 MHz compared to the experimental $|A^{55}_{Mn}|$ value of 263 MHz for a frozen solution of 50 μM Mn^{II} in 1 mM pH 7 orthophosphate. The calculated values for OxdC, which has three histidines in a facial configuration, and the related 3f structure were essentially the same. It was not possible to simply scale the calculated values, as has been done in other cases,[35] because the DFT calculations globally underestimated $|A^{55}_{Mn}|$ but overestimated the range of values spanned by the imidazole complexes. Nonetheless, the

use of large exact-exchange admixtures appeared to give A^{55}_{Mn} that were semiquantitative.

The ^{14}N isotropic hyperfine couplings ranged from 1.2 to 3.5 MHz; the lowest values belonged to the two four-coordinate models. The six-coordinate values were very close to the 3.2 MHz value measured for crystals[19] and the 2.7 MHz splitting observed in the PELDOR-NMR spectra. Hence, there was a high degree of consistency between the experimental measurements and DFT calculations not only for the hyperfine interactions but also for the structures of the complexes.

The calculated B95LYP/9s7p4d g values were all essentially isotropic and ranged from 1.9844 for $[Mn(H_2O)_6]^{2+}$ to 1.9792 for $[Mn(imidazole)_4]^{2+}$, greatly overestimating the range by a factor of 20, and were significantly offset compared to the measured values. This likely reflected the inadequacies of the effective nuclear charge (Z_{eff}) approximation used in Gaussian09 to calculate the spin−orbit contributions. By contrast, Schinzel et al. achieved much closer results for $[Mn(H_2O)_6]^{2+}$ (2.0018) and ConA (2.0018) using the B70LYP functional but using an atomic mean-field approximation.[34]

■ DISCUSSION

The EPR data indicated that not all of the structures that were calculated exist in the frozen aqueous solutions. Only $[Mn(H_2O)_6]^{2+}$, $[Mn(imidazole)(H_2O)_5]^{2+}$, $[Mn(imidazole)_3(H_2O)]^{2+}$, $[Mn(imidazole)_2(H_2O)_4]^{2+}$, and $[Mn(imidazole)_4]^{2+}$ are present in significant amounts. DFT thermochemical calculations showed that the trans form of $[Mn(imidazole)_2(H_2O)_4]^{2+}$ (structure 2t) was only 2.0 kcal/mol more stable than the cis form (structure 2c), suggesting that they were both likely to be present. ENDOR ligand-counting results showed that at 500 mM imidazole the average number of ligands was three imidazoles and one water molecule. This did not arise from a mixture of comparable amounts of the $[Mn(imidazole)_2(H_2O)_4]^{2+}$ and $[Mn(imidazole)_4]^{2+}$ because the 500 mM and 1 M imidazole 285 GHz cw-HFEPR spectra were nearly identical, with only a small contribution from $[Mn(imidazole)_2(H_2O)_4]^{2+}$ (<20%; red and blue, respectively, in Figure 2A). The data also precluded any significant amounts of $[Mn(imidazole)_3(H_2O)_3]^{2+}$. The four-coordinate $[Mn(imidazole)_3(H_2O)]^{2+}$ 3t structure was calculated to be 14 kcal/mol more favorable than the six-coordinate 3f structure. Taken together, the simplest equilibria that account for experimental and theoretical data are shown in Scheme 1.

Scheme 1

$[Mn(H_2O)_6]^{2+} + imidazole \rightleftarrows [Mn(imidazole)(H_2O)_5]^{2+} + H_2O$ (1)

$[Mn(imidazole)(H_2O)_5]^{2+} + imidazole \rightleftarrows [Mn(imidazole)_2(H_2O)_4]^{2+} + H_2O$ (2)

$[Mn(imidazole)_2(H_2O)_4]^{2+} + imidazole \rightleftarrows [Mn(imidazole)_3(H_2O)]^{2+} + 3H_2O$ (3)

$[Mn(imidazole)_3(H_2O)]^{2+} + imidazole \rightleftarrows [Mn(imidazole)_4]^{2+} + H_2O$ (4)
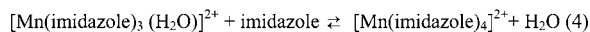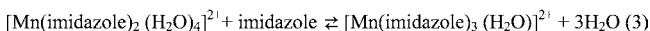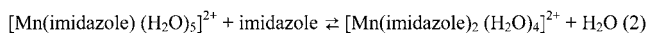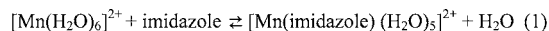
Because the free imidazole concentrations in the titration experiments (Figure 4) were always much higher than those of any other species, the apparent equilibrium constants for the four reactions could be obtained from the speciation data in a straightforward manner: $K_1 = 500 M^{-1}$, $K_2 = 150 M^{-1}$, $K_3 = 4.2 M^{-1}$, and $K_4 = 2.0 M^{-1}$. Because these values were obtained from frozen solution samples, they may not reflect the actual equilibrium constants.

When restricted to the Scheme 1 structures, the calculated spin parameters mirrored the experimental results. Although the B95LYP/9s7p4d g_{iso} values deviated strongly from the measured ones, the two, nonetheless, were strikingly linearly correlated (Figure 10A). This suggested that the calculated g values did have predictive value and provided corroboration of the measurements. The relationship between the calculated g_{iso} and $|A^{55}_{Mn}|$ values (Figure 10B) also followed the measured trend (Figure 3), as did the dependence of A^{55}_{Mn} on the number of imidazole ligands (Figure 9A). The calculated A^{55}_{Mn} values for $Mn(NH_3)_n(H_2O)_m]^{2+}$ complexes based on the BP86/TZVP combination also exhibited a similar dependence on the number of nitrogen ligands, although in this case, the values were underestimated by about a factor of 1.7, with the calculated values ranging from −155 MHz for $[Mn(H_2O)_6]^{2+}$ to −133 MHz for $Mn(NH_3)_6]^{2+}$.[36]

In terms of the charge distribution, progressing from zero to two imidazole ligands results in the positive charge of the manganese center decreasing, reflecting the increase in the electron delocalization due to the imidazoles. As a result, there is a reduction in the valence spin density. Munzarová and Kaupp have shown that this reduction in the spin population in the metal 3d orbitals will lead to a proportional decrease in the core−shell spin polarization and consequently a decrease in the metal isotropic hyperfine coupling.[37] In the context of the imidazole complexes, increasing the number of imidazole ligands leads to a reduction in the negative spin density of the core−shell, in particular the 2s orbital,[38] and as observed experimentally, a concomitant reduction in the size of A^{55}_{Mn}. Interestingly, the Mulliken spin densities, a global measure that includes both core and valence shell spin densities, increase but in such a way as to mimic the variation in A^{55}_{Mn}.

Changes in spin−orbital interactions were likely to be responsible for the linear dependence of g_{iso} on the number of imidazoles bound. Their effect on the g_{iso} values can be calculated using a second-order perturbation theory, which requires a summation of the matrix elements between the ground and excited states connected by spin−orbit coupling. Because the g_{iso} values were linearly related to A^{55}_{Mn}, this complex summation apparently is simply proportional to the Mn^{II} spin density. This appears to be confirmed by the calculated g_{iso} values (Figure 10). Such a simple behavior has been found to be true for simpler cases such as semiquinone radicals. Small shifts in their g values, for example, induced by hydrogen bonding, have been correlated to shifts in the spin densities of the oxygen atoms, where the bulk of the unpaired spin resides.[39] The underlying reason for this is that the largest spin−orbit contribution comes from the oxygen atoms of a semiquinone radical, which, in part, depends on the ground-state oxygen spin densities.[39] An analogous situation appears to exist in the case of the manganese(II) imidazole complexes. A greater ground-state manganese spin density resulting from the covalency of the manganese−imidazole bonding, as indicated by the Mulliken spin densities, results in an increasing departure from the free-electron g value (2.00232). Although the effects of ionicity on the ^{55}Mn hyperfine coupling were first demonstrated more than 50 years ago (for example, see ref 7), to the best of our knowledge, this is the first time it has been demonstrated for Mn^{II} g values. Interestingly, although the spin−orbital interactions are key components of both g values and zero-field interactions, their effect on the latter was not evident.
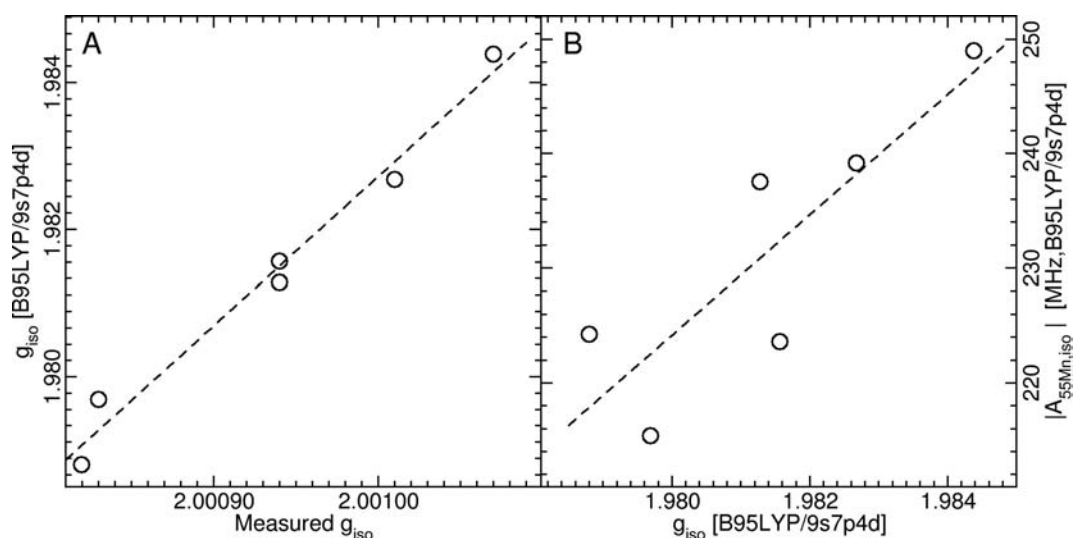
Figure 10. B95LYP/9s7p4d g_{iso} compared to (A) the measured g_{iso} values and (B) the B95LYP/9s7p4d $|A^{55}_{Mn,iso}|$ values. Calculated values have been restricted to the structures in Scheme 1. The dashed lines are linear regression fits.

The effect of imidazole covalency is considerable. The six-coordinate sites of OxdC (three histidines) and ConA (one histidine) have one and three carboxylate ligands, respectively, yet their hyperfine and g values are consistent with the corresponding pure imidazole–water ligand spheres. In contrast, an imidazole reduces the Mn^{II} charge to the same extent as a carboxylate. The Mn^{II} charges of ConA and OxdC are the same as the hypothetical $[Mn(imidazole)_4(H_2O)_2]^{2+}$ complex (Figure 9A). However, in solutions, this covalency effect is limited by the change from six- to four-coordinate geometry. This occurs when more than two imidazoles bond a Mn^{II} ion. This may reflect steric constraints due to the size of the imidazole molecule. Synthetically, the opposite appears to be true: only sterically constrained ligands yield four-coordinate Mn^{II} centers (see, for example, ref 40). The simple imidazole complexes existing in solution, as well as $[Mn(PO_4H_2)-(H_2O)_5]^+$, had calculated charges that were greater than 1.23, while the hypothetical structures with more than two imidazoles were lower. This suggests that, in addition to steric limits, there may be an optimal Mn^{II} charge range. However, as noted above, $[Mn(imidazole)_6]^{2+}$ does exist in crystals and has a A^{55}_{Mn} value of 240 MHz,[19] which approximately follows the same linear trend as the other six-coordinate molecules. This is also true for the three-imidazole OxdC center, which also has a coordinating glutamate. In this case, the total Mn^{II} charge is considerably lower, 1.15. If there is an optimal charge range, it may be overridden by other structural or environmental factors. It is interesting to speculate that constraining three imidazoles into a nontetrahedral geometry, such as in OxdC and MnSOD,[8] may induce a shift in the redox potentials of the Mn^{II} centers due to deficient charge.

In practical terms, the effect of imidazole ligation on ^{55}Mn isotropic hyperfine coupling, A^{55}_{Mn}, and g values that we have characterized can be used in a simple manner to test how many histidines or imidazoles, if any, are involved in a putative Mn^{II} binding site (Figure 3). Such a measurement on stationary growth phase *D. radiodurans* cells showed that over 40% of its Mn^{II} ions were characterized by an isotropic g value of 2.00098 $\pm$ 0.00004 with a ^{55}Mn hyperfine coupling of 256 $\pm$ 5 MHz, indicating that these ions were bound by two histidine residues of a peptide or protein (Figure 3). Small manganese(II) histidine complexes were unlikely because not only was there little cellular free histidine[41] but also two free histidines will only bind a single Mn^{II} ion in significant quantities at high nonphysiological pH (>8).[42] A six-coordinate complex is formed involving ligation to not only the two imidazole groups but also the two amino and carboxylate groups. This explained why the *D. radiodurans* HFEPR spectrum could not be reproduce with histidine at pH 7. Another large Mn^{II} fraction in *D. radiodurans* MnSOD.[3] This meant that over half of the Mn^{II} ions in *D. radiodurans* were bound to peptides or proteins, an unexpected result with potentially important consequences on how this remarkable organism survives high levels of radiation. Although such measurements can be done using conventional magnetic fields, higher magnetic fields will yield more accurate results.

■ ASSOCIATED CONTENT

Ⓢ Supporting Information

Additional figures showing ENDOR data of the proton and manganese regions together, a comparison of imidazole ENDOR spectra with different scaling, table of calculated hyperfine couplings and spin densities using different methods, and the full citation for the *Gaussian09* program. This material is available free of charge via the Internet at http://pubs.acs.org.

■ AUTHOR INFORMATION

Corresponding Author
*E-mail: sun.un@cea.fr.

Notes

The authors declare no competing financial interest.

■ ACKNOWLEDGMENTS

■ REFERENCES

(1) Golovin, A.; Henrick, K. *BMC Bioinf.* **2008**, *9*, 312.

(2) Daly, M. J.; Gaidamakova, E. K.; Matrosova, V. Y.; Vasilenko, A.; Zhai, M.; Venkateswaran, A.; Hess, M.; Omelchenko, M. V.; Kostandarithes, H. M.; Makarova, K. S.; Wackett, L. P.; Fredrickson, J. K.; Ghosal, D. *Science* **2004**, *306*, 1025.

(3) Tabares, L. C.; Un, S. *J. Biol. Chem.* **2013**, *288*, 5050.

(4) Deacon, A.; Gleichmann, T.; Kalb, A. J.; Price, H.; Raftery, J.; Bradbrook, G.; Yariv, J.; Helliwell, J. R. *J. Chem. Soc., Faraday Trans.* **1997**, *93*, 4305.

(5) Just, V. J.; Stevenson, C. E. M.; Bowater, L.; Tanner, A.; Lawson, D. M.; Bornemann, S. *J. Biol. Chem.* **2004**, *279*, 19867.

(6) Tabares, L. C.; Gatjens, J.; Hureau, C.; Burrell, M. R.; Bowater, L.; Pecoraro, V. L.; Bornemann, S.; Un, S. *J. Phys. Chem. B* **2009**, *113*, 9016.

(7) Matumura, O. *J. Phys. Soc. Jpn.* **1959**, *14*, 108.

(8) Tabares, L. C.; Gatjens, J.; Un, S. *Biochim. Biophys. Acta* **2010**, *1804*, 308.

(9) Bleany, B.; Rubins, R. S. *Proc. Phys. Soc. London* **1961**, *77*, 103.

(10) Bir, G. L. *Phys. Solid State* **1964**, *5*, 1628.

(11) Kliava, J. *Phys. Status Solidi B* **1986**, *134*, 411.

(12) Schosseler, P.; Wacker, T.; Schweiger, A. *Chem. Phys. Lett.* **1994**, *224*, 319.

(13) Gemperle, C.; Schweiger, A. *Chem. Rev.* **1991**, *91*, 1481.

(14) Carmieli, R.; Manikandan, P.; Kalb, A. J.; Goldfarb, D. *J. Am. Chem. Soc.* **2001**, *123*, 12438.

(15) Potapov, A.; Goldfarb, D. *Inorg. Chem.* **2008**, *47*, 10491.

(16) Raitsimring, A. M.; Astashkin, A. V.; Baute, D.; Goldfarb, D.; Poluektov, O. G.; Lowe, M. P.; Zech, S. G.; Caravan, P. *Phys. Chem. Chem. Phys.* **2006**, *7*, 1590.

(17) Rapatskiy, L.; Cox, N.; Savitsky, A.; Ames, W. M.; Sander, J.; Nowaczyk, M. M.; Rãgner, M.; Boussac, A.; Neese, F.; Messinger, J.; Lubitz, W. *J. Am. Chem. Soc.* **2012**, *134*, 16619.

(18) Florent, M.; Kaminker, I.; Nagarajan, V.; Goldfarb, D. *J. Magn. Reson.* **2011**, *210*, 192.

(19) Garcia-Rubio, I.; Angerhofer, A.; Schweiger, A. *J. Magn. Reson.* **2007**, *184*, 130.

(20) Un, S.; Dorlet, P.; Rutherford, A. W. *Appl. Magn. Reson.* **2001**, *21*, 341.

(21) Burghaus, O.; Plato, M.; Rohrer, M.; Möbius, K.; MacMillan, F.; Lubitz, W. *J. Phys. Chem.* **1993**, *97*, 1381.

(22) Davies, E. R. *Phys. Lett. A* **1974**, *47*, 1.

(23) Frisch, M. J. et al. *Gaussian09*, revision B0.01; 2010.

(24) Glendening, E. D.; Reed, A. E.; Carpenter, J. E.; Weinhold, F. *NBO*, version 3.1.

(25) Upreti, G. C. *J. Magn. Reson.* **1974**, *13*, 336.

(26) Epel, B.; Manikandan, P.; Kroneck, P. M. H.; Goldfarb, D. *Appl. Magn. Reson.* **2001**, *21*, 287.

(27) Carmieli, R.; Manikandan, P.; Epel, B.; Kalb (Gilboa), A. J.; Schnegg, A.; Savitsky, A.; Möbius, K.; Goldfarb, D. *Biochemistry* **2003**, *42*, 7863.

(28) Goldfarb, D.; Narasimhulu, K. V.; Carmieli, R. *Magn. Reson. Chem.* **2005**, *43*, S40.

(29) Stich, T. A.; Lahiri, S.; Yeagle, G.; Dicus, M.; Brynda, M.; Gunn, A.; Aznar, C.; Derose, V. J.; Britt, R. D. *Appl. Magn. Reson.* **2007**, *31*, 321.

(30) Garrett, T. P. J.; Guss, J. M.; Freeman, H. C. *Acta Crystallogr., Sect. C* **1983**, *39*, 1027.

(31) Garrett, T. P. J.; Guss, J. M.; Freeman, H. C. *Acta Crystallogr., Sect. C* **1983**, *39*, 1031.

(32) Yagüe, J. I.; Mohammed, A. M.; Loeffler, H.; Rode, B. M. *J. Phys. Chem. A* **2001**, *105*, 7646.

(33) Hedegärd, E. D.; Kongsted, J.; Sauer, S. P. A. *Phys. Chem. Chem. Phys.* **2012**, *14*, 10669.

(34) Schinzel, S.; Müller, R.; Kaupp, M. *Theor. Chem. Acc.* **2008**, *120*, 437.

(35) Sinnecker, S.; Neese, F.; Noodleman, L.; Lubitz, W. *J. Am. Chem. Soc.* **2004**, *126*, 2613.

(36) Duboc, C.; Collomb, M. N.; Pecaut, J.; Deronzier, A.; Neese, F. *Chemistry* **2008**, *14*, 6498.

(37) Munzarová, M.; Kaupp, M. *J. Phys. Chem. A* **1999**, *103*, 9966.

(38) Munzarová, M. L.; Kubáček, P.; Kaupp, M. *J. Am. Chem. Soc.* **2000**, *122*, 11900.

(39) Stone, A. J. *Mol. Phys.* **1963**, *6*, 509.

(40) Stibrany, R. T.; Lobanov, M. V.; Schugar, H. J.; Potenza, J. A. *Inorg. Chem.* **2004**, *43*, 1472.

(41) Daly, M. J.; Gaidamakova, E. K.; Matrosova, V. Y.; Kiang, J. G.; Fukumoto, R.; Lee, D.-Y.; Wehr, N. B.; Viteri, G. A.; Berlett, B. S.; Levine, R. L. *PLoS ONE* **2010**, *5*, e12570.

(42) Basosi, R.; Laschi, F.; Rossi, C. *J. Chem. Soc., Faraday Trans.* **1981**, *77*, 2361.

3813

dx.doi.org/10.1021/ic302415s | *Inorg. Chem.* 2013, 52, 3803−3813